HiSST: 2nd International Conference on
High-Speed Vehicle Science Technology
11–15 September 2022, Bruges, Belgium

Shock-Dominated Flow Control by Patterned Plasmas

Philip Andrews, Philip Lax, Sergey B Leonov[1]

Abstract

The results of an experimental study of shock-dominated flow controlled by a patterned electrical discharge are discussed. A solid wedge shock wave (SW) generator was installed in test section of M=4 wind tunnel. The Q-DC filamentary electrical discharge was arranged on the opposite wall so that the SW originating from the wedge impinged the area partially occupied with the plasma filaments arranged in a flow-wise direction with either a row of three filaments or only a single central filament. As a result of the SW-plasma interaction, the flowfield was significantly modified over the test section, including an upstream shift of the shock train. The details of the plasma-SW interaction, including the transitional effects, are explored with wall pressure measurements, schlieren imaging and Mie scattering visualization. The physics of the flow control effect is discussed.

Keywords: *Q-DC plasma, impinging SW, SWBLI, shock train control, Mie scattering*

1. Introduction

Control of shock-dominated flows is one of the major problems relevant to supersonic ducts, including scramjet flowpaths [1-2]. An effective air compression and low total pressure losses are achievable in the absence of a normal shock wave (SW) [3-5]. At off-design conditions the presence of a shock-shock interactions, shock-boundary-layer-interactions (SBLI), and combustion instabilities can result in engine unstart or in loss of thrust. The supersonic flow structure in the isolator and combustor is sensitive to the geometric configuration and main flow parameters, including the state of the boundary layer and structure of compression/expansion waves. This paper discuss the method for active control of the shock structure, potentially leading to maintenance of engine functionality in a wide range of external conditions. This method is based on the near-surface filamentary plasma generation being an alternative to passive control techniques such as stationary or movable mechanical elements, suction slots [6], vortex generators [7], or gas wall jets [8]. In contrast to a mechanical methods, a fast, inertia-free action can be provided by electrical discharges.

Along with several books and reviews [9-11], the feasibility of plasma-based techniques for steady and transient SW generation in supersonic flow has been demonstrated in several publications. Some works discussed a non-homogeneous plasma effect on SW position and pressure distribution volumetrically and over a plane wall [12-14] in a supersonic flow. In References [11, 14-15], the effect of filamentary plasma on SWs position in M=2 flow was described in details along with the discussion of the mechanism of interaction.

The mechanism of interaction and consequences of SW propagation in a temperature-stratified media were discussed in several computational works, in Refs. [12, 19, 20] for example. In the presence of a single heated gas filamentary zone, the SW front propagates far upstream compared to the SW in a cold gas due to a higher sonic velocity in the heated zone, as demonstrated in Fig. 1a. In the case of a heated filament realized in front of a blunt body in a supersonic flow, the SW structure significantly modified causing the drag reduction effect, see Fig. 1b. For a multifilamentary heated zone, or a "thermally stratified" media [20], the SW structure looks different compared to a single filament with the SWs forming a quasi-front of the propagating pressure jump. Such a gas heating pattern promises

[1] *Institute of Flow Physics and Control, University of Notre Dame, USA, sleonov@nd.edu*

benefits in terms of the energy magnitude needed for the expected control effect. However, a practical realization of a thermally-stratified zone in a free space is challenging.

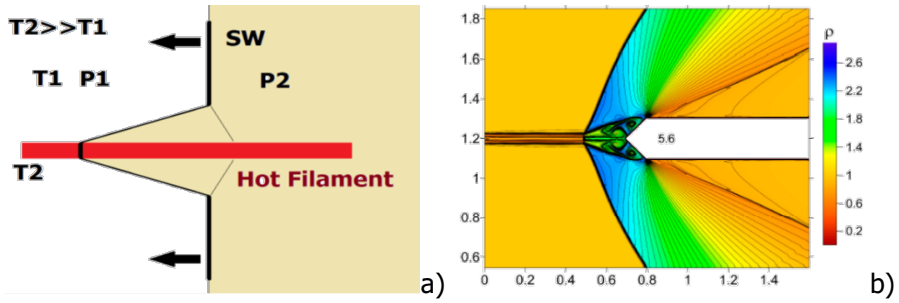

Fig 1. Illustration of the mechanism of SW interaction with thermally nonuniform layer: (a) schematics; (b) SW structure in front of blunt body with thermal filament [12]

At a near-surface electrical discharge excitation, plasma method of the flow control demonstrated a fast response at reasonably high actuation authority [15-18]. A specific structure of the near-surface gas layer, consisting of the intermittent lengthwise zones of supersonic and subsonic flow, also demonstrates a mitigating effect on an external impinging SW. In this study, one or three quasi-DC plasma filaments provide a rapid control of the shock train location and pressure distribution in a M = 4 duct with a compression ramp. The key finding considered in this work is the Mie-scattering visualization of a semi-conical SW appeared in supersonic flow is result of SW-BL-plasma interaction.

2. Description of the experimental arrangement

The test program were performed at the SBR-50 supersonic blowdown wind tunnel facility at the University of Notre Dame [21]. Operating conditions were as follows: flow Mach number M = 4, ambient stagnation temperatures, stagnation pressures P0=2.6-4 bar, and steady-state run time t> 1 sec. The test section has of a rectangular cross section of initial dimensions 76.2×76.2 mm with a 1° expansion on the top and bottom walls to compensate for boundary layer growth. A spanwise uniform 17° wedge is installed on the top wall of the test section to generate a planar shock wave impinging in the plasma region on the bottom wall, see Fig. 2a. The location of this shock impingement can be controlled by moving the wedge between three available locations as shown in the schematics. The plasma was generated using a quasi-DC electric discharge from three high voltage electrodes embedded in ceramic insert spaced 19mm apart from each other and from the side walls and located 149mm downstream of the nozzle exit. Two grounding rails of width 2.6mm were placed 19.05mm apart from each other and 28.5mm from the side walls in order to provide an initial breakdown and to elongate the plasma filaments as shown in Fig. 2b. The electrical discharge was generated using a custom capacitor-based power supply operating in a current stabilized mode at breakdown voltage in a range of U_{ps} = 4-5kV. Optical access was provided through quartz side windows. The image of the bottom insert construction, including the electrodes' system and pressure ports, is presented in Fig. 2b.

For this test series, the basic instrumentation includes pressure measurements, schlieren imaging, high speed plasma imaging, spectroscopic observations, and electrical measurements. Static pressure data over the test section are measured using a 64-channel pressure scanner (Scanivalve MPS4264) with an acquisition frequency of 800Hz collecting from 48 possible pressure locations on the top and bottom walls. Pressure measurements are also taken across a span perpendicular to flow along the bottom wall in the plasma generation region to investigate the effect of generated plasma on the flow structure. Two rows of pressure taps at 165.5mm and 180.7mm downstream from the nozzle with 4.57mm spacing between each tap recorded the crossflow static pressure. Kulite pressure sensors with a sample rate of 80000samp/sec were installed at key locations in the top wall in the vicinity of the reflected shock impact to study the dynamics of shock movement. The schlieren arrangement consists of a high current pulsed white LED light source (100ns pulse duration) and Phantom v2512 high speed camera operating with a framerate of 1kHz and exposure of 1.25μs. Plasma imaging was also performed with the Photron Nova S9 FastCam collecting with an exposure of 12.5µs and 20kHz framerate. Electrical probes were used to measure gap voltages, current and, then, to calculate electrical power deposition. Typical electrical parameters for each filament are as follow: gap voltage U_{pl} = 0.1-0.3 kV, electric current I=2-4.5A and plasma power W_{pl} = 0.5-1.0 kW. Gas temperature in plasma was measured by optical emission spectroscopy of second positive system of molecular nitrogen (Ocean Optics

spectrometers), it was T_g=3-5kK, T_v=6.5-7.5 kK depending on the electric current through the discharge.

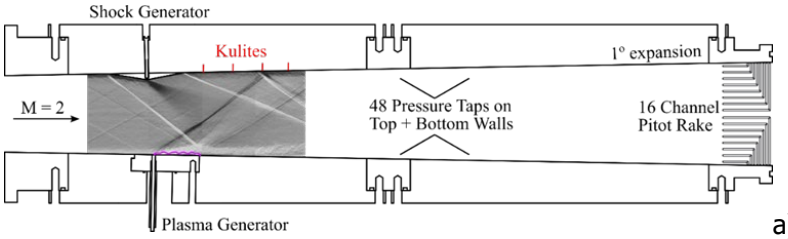

a)

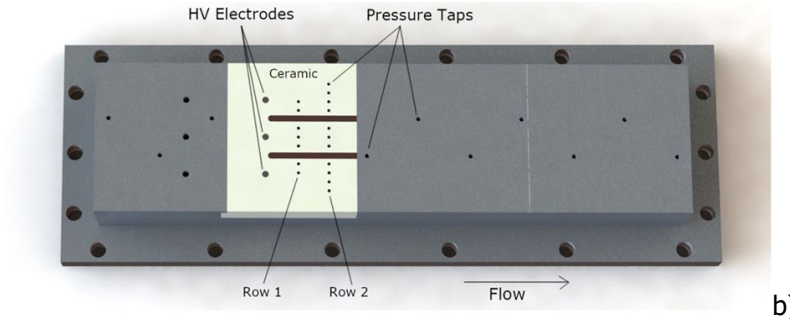

b)

Fig 2. SBR-50 facility test arrangement: (a) side view cross-section; (b) image of the bottom insert.

3. Experimental results

3.1. Electrical discharge appearance and dynamics

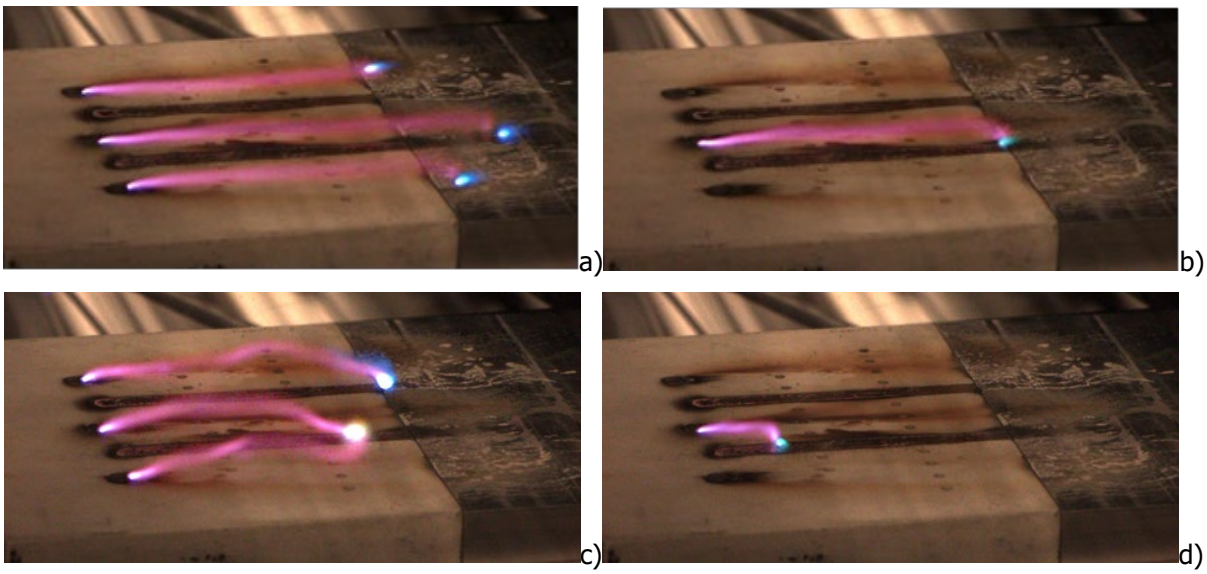

a) b) c) d)

Fig 3. High speed image of plasma filaments an exposure time of 4μs without (a,b) and with (c,d) shock wave impingement: triple plasma filaments (a,c) vs single one (b,d). Flow from left to right

The first test series aimed at to characterize the plasma geometry and the effect of an impingent shock on the plasma morphology. During steady state flow in each run, three-to-five plasma pulses were activated at 10Hz repetition rate with a 30ms duration of each pulse. Figure 2 presents a typical plasma filaments images for the case when an impingent shock absent and is present. The images comparison is consistently demonstrating that, with an impingent shock present, the plasma filaments are highly perturbed from their otherwise linear shape. This happens due to presence of an extensive flow separation zone generated in result of the impinging SW and plasma interaction [16], which is well visible in the schlieren images in Figs. 4b and 4d. The single filament can elongate by grounding to either rail and thus its exact position at a given time is largely stochastic. Furthermore, the high pressure

zone of the impinging shock consistently prevents the single plasma filament from fully elongating past the position of the impingent SW.

3.2. Schlieren visualization

Followed testing was focused on the plasma effect on the flow structure. The schlieren imaging demonstrated that the basic effect of plasma actuation on the ramp-generated shock train and on the flow-field structure is seen in two key regions: (1) compression wedge shock impact on the plasma array and (2) the reflection of this shock back to the upper wall. Figure 4 presents schlieren images stitched together across the region of interest in the test section. Images collected prior to the plasma being turned on are shown in Figs. 4a and 4c and images during plasma actuation are shown in Fig. 4 for a single plasma filament (a,b) vs triple filaments setup (c,d). Before plasma is activated, the flowfield is dominated by a strong shock from the leading edge of the compression wedge, expansion fan from the top of the wedge (visible as a black fan after the impinging SW), and the end shock from the ramp back wedge. The first reflection of the leading edge oblique shock from the bottom wall is seen near the center of Figs. 4a and 4c. After extended plasma forms over the bottom wall, the reflection of the shock impinging on the plasma array is largely mitigated, and a new shock forms upstream at the location of the high voltage electrodes, as it is demonstrated in Figs. 4b and 4d. This causes upstream movement of the whole shock train. In Figure 4b, this new SW pattern is less visible die to a single plasma filament induce a semi-conical SW occupied only a portion of the span-wise distance. The effect of plasma on shock structure configuration is reflected in wall pressure distribution showing the shift of the shock wave position upstream.

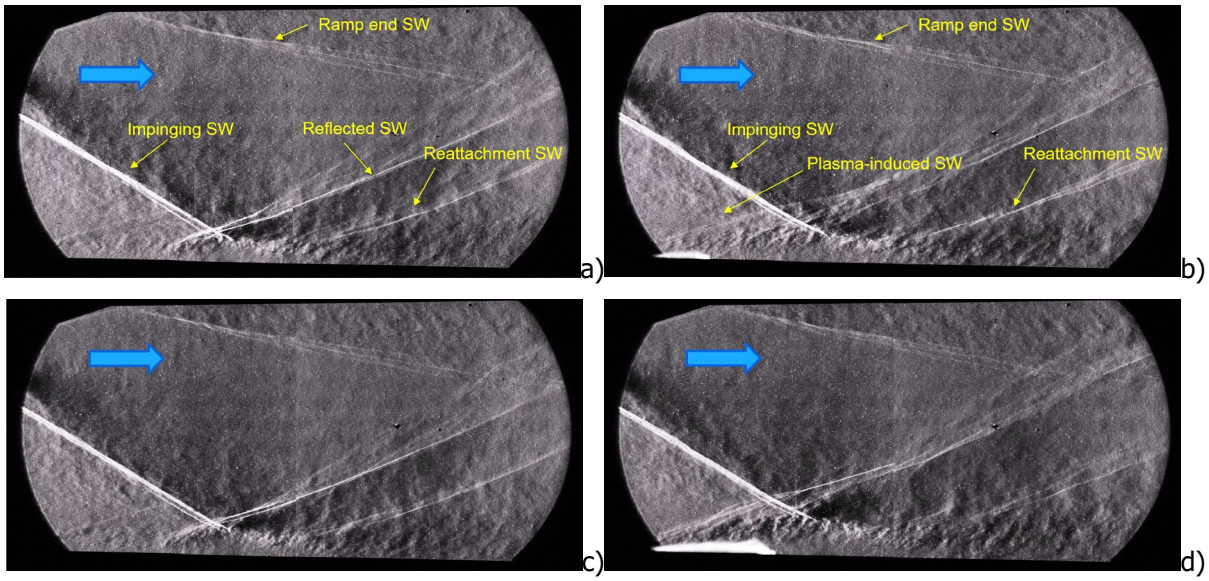

Fig 4. Schlieren images collected at P0 = 1.7 bar where (a) shows a no plasma case and (b) shows a plasma on case at a single plasma filament power Wpl = 2.1 kW.

3.3. Pressure measurements

The effect of plasma on shock structure configuration is well reflected in pressure data taken from the two rows of pressure taps arranged perpendicular to the flow as well as static pressure ports along the top/bottom walls. Examining the two perpendicular rows of sensors in the plasma region reveals a movement of existing shocks upstream and the cross-sectional structure for the single filament case. Pressure distribution profiles from row 2 are shown graphed across three plasma pulses in time are included in Fig. 5.

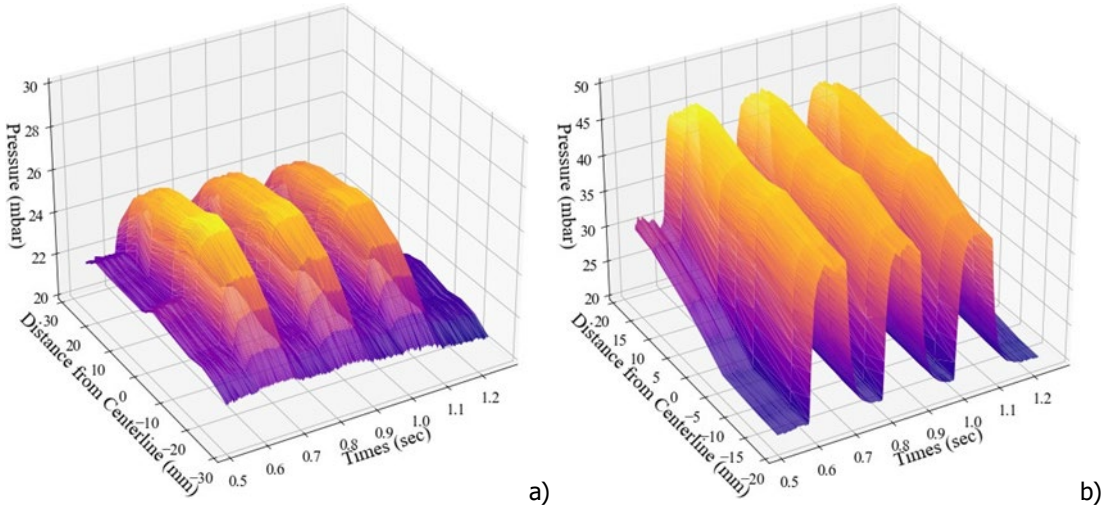

Fig 5. Time series of row 2 pressure distribution during three consecutive plasma pulses at P_0 = 2.6bar comparing pressure redistribution between (a) single filament and (b) three filaments actuation.

When plasma is actuated on, rapid near-adiabatic heating creates a localized subsonic region which causes an upstream movement of the existing shock so that a new shock is generated starting at the plasma electrodes location. Thus, pressure taps in both rows are now behind the new shock and exhibit increased pressure. Collected data demonstrates that in the case of single plasma filament test, pressure increases primarily along the centerline, in the region local to the single filament whereas with three filaments the pressure rises more uniformly across the entire row. Absolute changes in pressure are significantly lower at Mach 4 than at Mach 2 [18] due to the much lower density flow, but the relative strength of pressure redistribution is similar. Data for the single filament case provides clear evidence of the semi-conical pressure redistribution caused by an increase in pressure local to just the central single filament. With the wedge removed and no existing shock train present, pressure effect is much weaker which indicates that the plasma filament acts as a subsonic channel for existing SWs but does not generate its own strong SW.

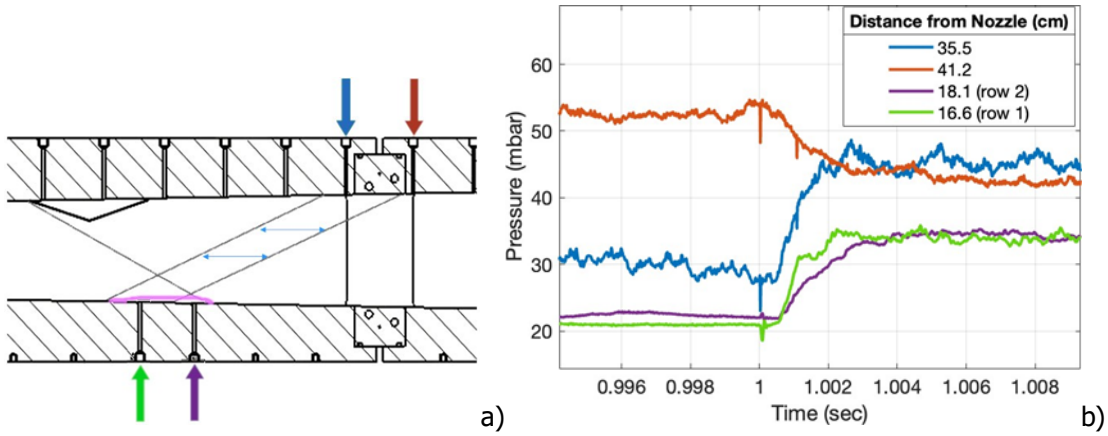

Fig 6. (a) Locations of Kulite sensors; (b) pressure dynamics at each location when plasma is turned on at t = 1sec

By looking at key pressure ports along the top wall where the reflected shock is impinging, pressure data can corroborate the movement of the shock train displayed in schlieren images. Using Kulite sensors also provides time-resolved data quantifying the dynamics of the shock train position via this pressure redistribution. Figure 6 provides the location of installed sensors and the pressure dynamics at those tap locations. As the reflected shock impacting the top wall moves upstream due to plasma actuation, the pressure at x = 35.5cm on the top wall dramatically increases indicating this sensor is now located behind the new shock front whereas the pressure at x = 41.2cm decreases suddenly since the reflected SW is no longer directly impinging. Likewise, both locations in the plasma region experience a rapid jump in pressure as the SW shifts upstream.

There is a short delay of about Δt=250μs before any pressure effect is registered: this occurs during plasma formation and elongation by the flow. Downstream pressure ports then indicate a change in pressure before the front arrives upstream and stabilizes. The time delay after plasma is turned on to fully establish the new SW pattern and pressure distribution is about Δt=1ms. A reverse effect occurs where upstream pressure drops before downstream pressures change, and after about Δt=1ms pressures return to their original stable baseline levels. Between all Kulite locations, there is agreement that redistribution of the shock train occurs in <2ms.

3.4. Flow structure details by Mie scattering

While schlieren images provide excellent visualization of stream-wise features of SW-plasma interaction, Mie scattering was used to probe the cross-flow SW structure when the impingent SW interacts with a single plasma filament. Images were collected at an angle through the side windows of the tunnel and a known calibration grid image was used to apply a projective transform and extract quantitative dimensions from the resulting orthogonal view. In this work, planar laser Mie scattering is applied to qualitatively map condensation in a cold M=4 flow, visualizing the SWs, BLs, and zones with gas density variation or gas temperature variation. As the bulk air is seeded with CO2 in amount up to 7% in number density, significant condensation can occur. In this work 2nd harmonic of a Solar Laser Systems Nd:Yag laser at 532nm with a pulse repetition frequency of 100Hz, pulse width of 10ns, and average pulse energy of 60mJ was used. For the spanwise laser sheet arrangements, traditional two lens sheet forming scheme was applied. This consisted of a spherical plano-convex lens (f = 500mm) and a cylindrical plano-concave lens (f = -100mm) which provided a collimated laser sheet of height h = 76.2mm and thickness of approximately w = 0.500 mm at the center-line of the test section. Image acquisition was performed using intensified relay optics (LaVision 1102080) coupled to a Basler (acA2040-180km) camera. Intensifier exposure time was fixed at 500ns and the Basler camera exposure was set to 2ms to capture the signal decay from the P43 phosphor in the intensifier. Image acquisitions were timed off the q-switch of the laser and collected at 100Hz.

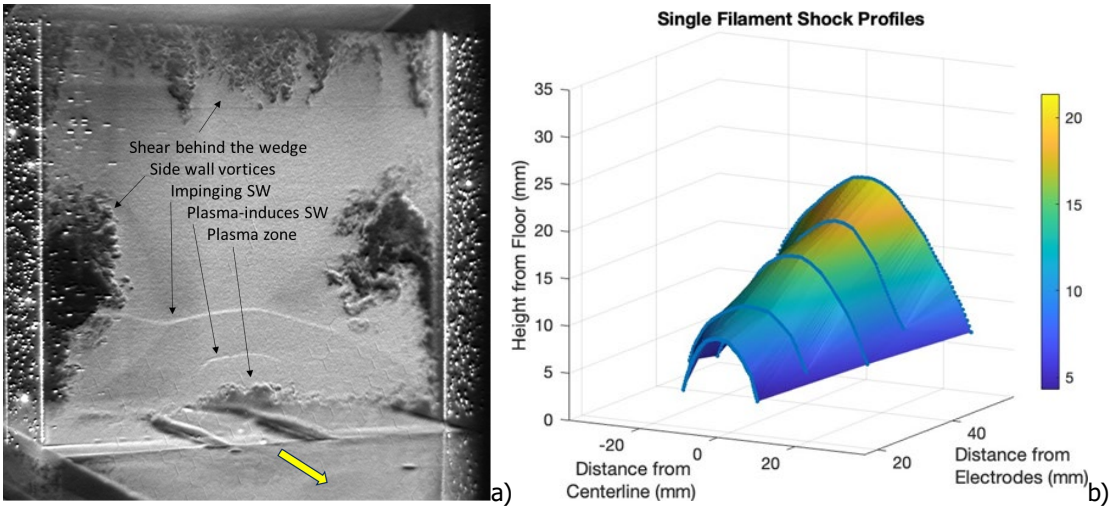

Fig 7. An example of Mie scattering image (a) and the resulting SW profile merged from a multi-layer scanning at single plasma filament case (b).

It is assumed that the intensity of scattered light corresponds to the number of droplets and thus is a function of the local gas density and temperature. In Mie scattering images, oblique SWs appear as bright lines that mark the transition between dimmer regions upstream of the shock and slightly brighter regions behind the SW. Thus, by scanning the laser sheet across the region of interaction, the cross-flow profiles of the plasma generated SW was mapped out. Figure 7 illustrates the image example collected at laser sheet position x= 30mm from the electrode, Fig. 7a as well as the final 3D surface generated by merging each of the shock profiles together, Fig. 7b. There are many details of the flow structure acquired by Mie scattering and visible in Fig. 7a, including the impinging SW interaction with side walls and side walls vortices, which are normally can't be retrieved from schlieren images. Each side wall vortex strongly interacts with the wedge generated compression SW, but it is still unknown if they have any impact on the plasma-SW interaction. The resulting SW surface matches predictions of a semi-conical SW due to a localized subsonic channel around the plasma filament. The SW is assumed to

originate from the plasma electrode, however, visualization is challenging within the turbulent boundary layer since increased heating causes droplets to re-evaporate.

4. Discussion

In accordance with the model of interaction and the data acquired for a single plasma filament, theory and simulation predicts a semi-cone shape of the plasma-induced SW with a zone of augmented pressure within that cone and a significantly lower pressure outside of it. In the case of multi-filamentary plasma array, the individual SWs interference leads to almost planar plasma-induced SW appearance, which is considered to be equivalent to shifting of the entire shock train upstream. This predicted effect was now demonstrated experimentally at M=4 by analysis of cross-flow pressure distribution for single and triple plasma filament configurations as well as through carbon dioxide Mie scattering visualization.

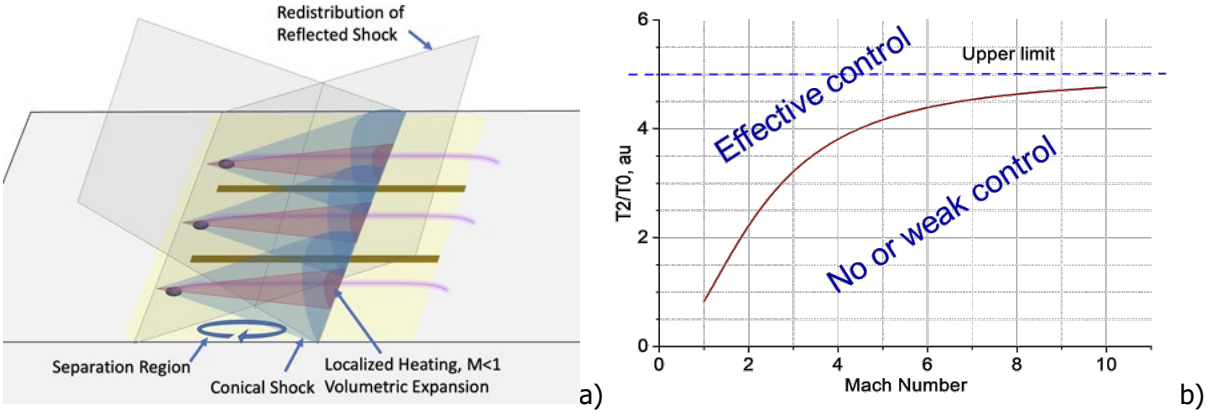

Fig 8. Illustration of SW-BL-plasma interaction (a); simplified criteria of plasma control of SW position (b).

The filamentary plasma authority for the SW position control is well confirmed experimentally for a variety of conditions [11, 15, 17-18], including M=2 and M=4 supersonic flows. The mechanism of interaction is understood to be essentially thermal as illustrated in Fig.8a and is formulated as follows: With a high local gas temperature, the multi-filamentary plasma zone presents an array of longitudinal subsonic jets surrounded by a supersonic flow. The volumetrically expanded zone produces a long cone of subsonic flow, where the physical velocity is close to the gas speed in the supersonic core flow. Such an uncommon gasdynamic structure produces a near-surface stratified zone, which enables a significant redistribution of the gas pressure. The pressure bump associated with an impinging SW is mitigated and moves upstream until reaching the electrode locations. The reversal x-gradient of pressure is reduced significantly. Such a redistribution of the gas pressure leads to a visible mitigation of the reflected SW and looks like the appearance of a new SW originating from the electrodes' area.

Based on the mechanism of SW-BL-plasma interaction, a simplified criterion of effective SW position control can be proposed assuming the following conditions: $M2 < 1$ – Mach number in plasma filaments and immediately surrounded area M2; and $V2 \approx V1$ – physical gas velocity inside the plasma filament is about the external flow velocity [15]. With such speculations, the gas temperature T2 in plasma channel should satisfy the following expression:

$$T2 > T_0 \cdot \left(\frac{1}{M^2} + \frac{\gamma-1}{2}\right)^{-1},$$

where T_0 is stagnation gas temperature in external flow with Mach number M. For example, for M=2 the temperature $T2 > 2.2\ T_0$; for M=4 $T2 > 3.8\ T_0$. The criterion is shown graphically in Fig. 8b; the curve coming to a $T2/T_0=5$ limit at high Mach number. The criterion is well-achievable at low T0 but could be challenging at higher temperatures, T_0>1kK for example.

This described method of the SW position control is a paradigm-shifting concept where plasma is used for an active triggering action whereby narrow subsonic channels are opened for the pressure drain into an upstream area in supersonic or hypersonic flows such that a very small energy deposition relative to existing flow power leads to a significant redistribution.

5. Concluding remarks

The results of experimental study are discussed on a filamentary plasma effect on a shock-dominated flow in a rectangular duct. Mitigation of the reflected SW from the ramp is observed in schlieren images, along with the formation of a new oblique SW at the location of electrodes. This leads to the formation of a new SW train throughout the test duct, shifted further upstream from the previous pattern.

Based on schlieren visualization, pressure measurements, and Mie scattering visualization, the major findings of this work are new details of a SW - plasma array/single filament interaction including the shape of the plasma-induced semi-conical SW and the dynamics of the plasma-induced SW. Fast pressure sensor measurements determined a delay time of <1ms after plasma actuation for this new SW train to fully establish, with a similar time to return to baseline flow when actuated off.

The experimental data analysis allows for the formulation of a thermal mechanism of interaction and a simplified criterion of the effective control of the SW position. Based on this, the critical plasma temperature for the triggering effect to work is a rising function of the flow Mach number. It is also concluded that the method might be especially effective for a cold external flow.

Acknowledgments
The authors appreciate the US Air Force Office of Scientific Research (PM Dr. Gregg Abate) for funding this work, grant # FA9550-21-1-0006.

References

1. N. T. Clemens and V. Narayanaswamy, "Low-Frequency Unsteadiness of Shock Wave/Turbulent Boundary Layer Interactions," Annual Review of Fluid Mechanics, vol. 46, pp. 14-46, 2014.
2. K. Matsuo, Y. Miyazato and H. Kim, "Shock train and pseudoshock phenomena in internal gas flows," Prog. Aerosp. Sci., vol. 35, pp. 33-100, 1999.
3. J. Seddon and E. L. Goldsmith, Intake Aerodynamics, 2nd edition ed., AIAA Education Series, 1999.
4. L. E. Surber and J. A. Tinapple, ". 2012. Inlet Flow Control Technology: Learning from History, Reinventing the Future," AIAA Paper 2012-0012, 2012.
5. D. S. Dolling, "Fifty Years of Shock-Wave/Boundary-Layer Interaction Research: What Next?," AIAA Journal, vol. 39, no. 8, 2001.
6. A. Weiss and H. Olivier, "Shock boundary layer interaction under the influence of a normal suction slot," Shock Waves, vol. 24, pp. 11-19, 2014.
7. A. Valdivia, K. B. Yuceil, J. L. Wagner, N. T. Clemens and D. S. Dolling, ""Control of supersonic inlet-isolator unstart using active and passive vortex generators," AIAA Journal, vol. 52, no. 6, pp. 1207-1218, 2014.
8. H. Do, S. Im, M. Mungal and M. Cappelli, "The influence of boundary layers on supersonic inlet flow unstart induced by mass injection," Exp. Fluids, vol. 51, pp. 679-691, 2011.
9. D. Knight, "Survey of Aerodynamic Drag Reduction at High Speed by Energy Deposition," Journal of Propulsion and Power, vol. 24, no. 6, p. 1153–1167, 2008.
10. A. Starikovskiy and N. Aleksandrov, Nonequilibrium Plasma Aerodynamics, Aeronautics and Astronautics, Max Mulder (Ed.): InTech, ISBN: 978-953-307-473-3, 2011.
11. S. B. Leonov, I. V. Adamovich and V. R. Soloviev, "Dynamics of near-surface electric discharges and mechanisms of their interaction with the airflow, Topical Review," Plasma Sources Science and Technology, vol. 25, no. 6, p. 20168, 2016.
12. O. A. Azarova, T. A. Lapushkina, K. V. Krasnobaev, O. V. Kravchenko, "Redistribution of Energy during Interaction of a Shock Wave with a Temperature Layered Plasma Region at Hypersonic Speeds", Aerospace, 2021, 8(11), 326.
13. S. Leonov, V. Bityurin, A. Klimov and Y. Kolesnichenko, "Influence of Structural Electric Discharges on Parameters of Streamlined Bodies in Airflow," AIAA Paper 2001-3057, 2001.
14. F. Falempin, A. Firsov, D. Yarantsev, M. Goldfeld, K. Timofeev and S. Leonov, "Plasma control of shock wave configuration in off-design mode of M = 2 inlet," Experiments in Fluids, vol. 56, no. 54, 2015.
15. A. Houpt, B. Hedlund, S. Leonov, T. Ombrello and C. Carter, " Quasi-DC Electrical Discharge Characterization in a Supersonic Flow," Experiments in Fluids, vol. 58, no. 4, p. 25, 2017.

16. S. Elliott, P. Lax and S. Leonov, "Realignment of Shock Wave Reflection Pattern by Plasma Array," AIAA Paper 2021-3116, 2021.
17. Y. Watanabe, S. Elliott, A. Firsov, A. Houpt, S. Leonov, "Rapid control of force/momentum on a model ramp by quasi-DC plasma," J. Phys. D: Appl. Phys., vol. 52, #144, p. 444003, 2019.
18. S. Elliott, P. Andrews, P. Lax and S. B. Leonov, "Control of Shock Positions in a Supersonic Duct by Plasma Array," AIAA Paper 2022-2553, 2022.
19. O. Azarova, «Supersonic Flow Control Using Combined Energy Deposition,» Aerospace, vol. 2, #11, pp. 118-134, 2015.
20. V. Bityurin, A. Klimov, S. Leonov, D. V. Wie, V. Brovkin, Y. Kolesnichenko et A. Lutsky, «Effect of heterogeneous discharge plasma on shock wave structure and propagation,» AIAA Paper 1999-4940, https://doi.org/10.2514/6.1999-4940, 1999.
21. P. Andrews, P. Lax, S. Elliott, A. Firsov and S. Leonov, "Flow Characterization at Heated Air Supersonic Facility SBR-50," Fluids, vol. 7, #15, p. 168, 2022.